International Journal of Disaster Risk Reduction 145 (2026) 106410

Contents lists available at ScienceDirect

International Journal of Disaster Risk Reduction

journal homepage: www.elsevier.com/locate/ijdrr

Assessing the consequences of compound coastal–fluvial flooding under climate change: exposure, vulnerability and damage estimates in eastern England

Ross Gudde [a], Yi He [a,*], Ulysse Pasquier [a], Paul B. Sayers [b]

[a] *Tyndall Centre for Climate Change Research, School of Environmental Sciences, University of East Anglia, UK*
[b] *Sayers and Partners LLP, Oxfordshire, UK*

ARTICLE INFO

Keywords:
Flood
Risk
Hazard
Exposure
Vulnerability
Climate

ABSTRACT

Flood risk is projected to increase under climate change due to more frequent extreme events and expanding human development in hazard-prone areas. While large-scale assessments provide valuable overviews of emerging risk, they often lack the spatial detail and social-environmental integration needed to inform local adaptation planning. This study applies a high-resolution hazard-exposure-vulnerability framework to assess compound coastal–fluvial flood risk and evaluates how methodological choices affect estimates of exposure, economic damage and spatial risk. The framework is applied to the low-lying Broadland catchment in eastern England using UKCP18 convection-permitting climate projections under RCP8.5 to simulate compound flood scenarios for 1990, 2030, and 2070. Exposure is assessed using population and property data, while vulnerability is quantified across 31 social, economic, and environmental indicators statistically weighted via principal components analysis. The results show that methodological choices can substantially influence outcomes. In particular, building depth sampling methods and depth–damage assumptions can alter loss estimates by over 70%, while different population datasets affect estimated human exposure. By using the OpenPopGrid population dataset and the footprint-maximum depth, the estimated economic damages increase from £439 million in 1990 to £718 million in 2070, with risk concentrated in urban coastal locations where exposure and vulnerability converge. By integrating high-resolution climate projections with spatially explicit vulnerability analysis, this study demonstrates how local-scale assessments can provide spatially detailed evidence to inform adaptation planning. The framework is potentially transferable to other coastal and estuarine regions, although its implementation depends on the availability and local suitability of hazard, exposure and vulnerability data.

1. Introduction

Traditional definitions of flood risk consider both the likelihood and adverse consequences of inundation on an asset or system [3, 4]. This is commonly represented through the "risk triangle" of hazard, exposure and vulnerability [5,6]. Hazard refers to the probability and magnitude of a potentially damaging event, exposure to the presence of people, infrastructure or environmental systems in places that could be affected, and vulnerability to the susceptibility of those elements to harm and their capacity for loss [7–9]. While

* Corresponding author.
E-mail address: yi.he@uea.ac.uk (Y. He).

https://doi.org/10.1016/j.ijdrr.2026.106410
Received 20 April 2026; Received in revised form 31 August 2026; Accepted 1 September 2026
Available online 4 September 2026

this hazard–exposure–vulnerability framing is well established, its practical implementation remains sensitive to data choice, spatial scale, indicator selection and damage-estimation assumptions, particularly for compound flood events.

Flooding is historically one of the most impactful natural hazards in the UK, with major events including the 1953 North Sea flood, the 2007 summer floods and the 2013/14 winter floods causing severe social and economic impacts [10–12]. The potential to experience loss from such events is not uniform, as previous studies on social vulnerability have shown (e.g. Ref. [13]).

While future flood risk is often framed in terms of increasing hazard intensity due to climate change, changes in exposure and vulnerability may further compound these risks. Exposure is likely to increase, with continued population growth, increasing urbanisation and floodplain development (e.g. Ref. [13–17]). The third UK Climate Change Risk Assessment (CCRA) estimates 544,000 residential and 72,000 non-residential buildings are situated on coastal floodplains [18]. Of these, approximately 47,000 residential and 11,000 non-residential buildings are subject to an average rate of flooding of less than 1-in-75-years (ibid). With limited adaptation in flood risk management, these exposure magnitudes are estimated to increase by six-to ten-fold in UK residential properties under 2 and 4°C warming futures by 2100, respectively (ibid). The exposure of vulnerable populations is also projected to increase disproportionately, with the population in flood-prone areas rising by 45% to 10.8 million, while the increase in deprived neighbourhoods is projected to reach 310%, from 451,000 to 1.4 million [13].

The Norfolk and Suffolk Broads in East Anglia represent a low-lying, flood-prone region, where land sits at or below sea level with a tidal-dominance from the North Sea reaching 40-50 km inland (CH2M, [19–21]). The wider Broadland catchment includes a dense river network, making the region susceptible to both tidal and fluvial flooding [20]. Over the years, flood risk management has become more strategic, with Shoreline Management Plans (SMPs) being implemented and flood compartments separating low-elevation land into 40 distinct segments ([22,23]; CH2M, 2016). However, despite proposals for more future-focused strategies, many areas continue to follow a 'hold-the-line' approach [24–26].

Integrated flood-risk assessment encompasses a range of approaches that differ in their treatment of hazard, exposure, vulnerability and consequences. Some studies focus primarily on the spatial distribution of inundation, exposed assets and direct economic damage. For example, Thumerer et al. [27] estimated potential damage across land-use classes, while Mokrech et al. [28] examined how socio-economic development pathways could alter future coastal-flood exposure in eastern England. Such approaches provide direct estimates of physical and economic consequences but may represent social vulnerability only indirectly. A second strand of research uses indicator-based methods to characterise the susceptibility and coping capacity of exposed populations. Shepard et al. [29] combined exposure and vulnerability in assessing coastal-flood risk, while Garbutt et al. [30] developed social-vulnerability indices for Norfolk based on population sensitivity, access to services and flood-hazard zones. Scheuer et al. [31] and Kotzee and Reyers [32] extended this perspective through multidimensional composite indices incorporating social, economic and environmental indicators. These methods can identify spatial inequalities in vulnerability, although their results depend on indicator selection, weighting and spatial aggregation. Other integrated frameworks combine hazard, exposure and vulnerability within a common spatial assessment. These approaches range from relatively transparent index-based methods to probabilistic risk models and system-based decision--support frameworks. They differ in whether risk is represented through expected annual losses, scenario-specific impacts, composite indices, or robustness across multiple futures. The appropriate approach therefore depends on the decision context, available data and required spatial and probabilistic detail.

The present study falls within the third category of integrated hazard–exposure–vulnerability assessment and applies this established approach to a high-resolution compound coastal–fluvial flood assessment in the Broadland catchment. Building on the compound flood hazard modelling presented by Gudde et al. [2], it links scenario-specific inundation with population exposure, building-level direct-damage estimates and an MSOA-level multidimensional vulnerability index. The overarching aim is to assess climate-driven compound flood risk while evaluating how selected data choices and analytical assumptions influence estimates of population exposure, economic loss and spatial risk prioritisation.

Specifically, the study addresses three research questions: (1) how can compound flood risk be spatially characterised at fine resolution by integrating high-resolution hazard projections with multi-dimensional exposure and vulnerability metrics; (2) how are flood risks projected to evolve over time under UKCP18 convection-permitting climate scenarios; and (3) how do methodological choices, such as population datasets, exposure thresholds, building-depth sampling methods and depth-damage assumptions, influence estimates of future flood risk?

To address these questions, the study combines UKCP18 convection-permitting model (CPM) climate projections with spatially explicit exposure mapping and multidimensional vulnerability analysis for the Broadland catchment, UK. It links compound coastal–fluvial inundation scenarios with population and building exposure datasets, economic damage estimation and a vulnerability index that incorporates social, economic and environmental indicators. The resulting assessment provides locally relevant evidence to inform adaptation and disaster-risk-reduction planning. The spatial risk patterns are intended to support screening and prioritisation for more detailed place-based assessment rather than evaluation of specific adaptation measures.

2. Data and methodology

This flood risk assessment follows the "risk triangle" framework, in which risk is conceptualised as the interaction of hazard, exposure, and vulnerability. Hazard is characterised using high-resolution compound fluvial–tidal inundation scenarios derived from the hydrodynamic modelling of Gudde et al. [2], driven by UKCP18 RCP8.5 projections. Exposure is quantified for both population and buildings by overlaying flood-depth rasters with gridded population datasets and a building footprint inventory. Vulnerability is represented by a composite index of social, economic, and environmental indicators, with indicator weights derived using principal components analysis (PCA). The overall workflow and associated input datasets are summarised in Fig. 1. In addition to producing scenario-specific risk estimates, the workflow was also designed to examine how selected methodological choices influence exposure and damage estimates, including population dataset selection, flood-depth thresholding, building-depth sampling and depth–damage assumptions.

2.1. Study area

The Broadland catchment in East Anglia, UK, spans approximately 3200 km^2 with nearly 1 million residents across villages, towns and 13 major settlements (Fig. 2); the three largest being Norwich, Great Yarmouth and Lowestoft [33–35]. It is drained by five primary rivers, the Ant, Bure, Wensum, Yare and Waveney, which converge in the Broads National Park before discharging into the North Sea [33]. This Broadland catchment features 107 Middle Super Output Areas (MSOAs) as of the 2021 UK Census. Each MSOA represents a disaggregated segment of local authorities and contains approximately 2000–6000 households with a resident population of 5000–15,000 [36]. MSOAs were selected as the common reporting unit in this study because they represented the finest spatial scale at which the full suite of social, economic and environmental indicators could be assembled consistently. Population exposure was estimated by overlaying each gridded population dataset with the 2 m flood-depth rasters, while building exposure was assessed at building-centroid or building-footprint scale. The population exposure was aggregated to MSOA level for integration with vulnerability.

At 303 km^2 with 2.7 km of coastline, the Broads National Park is the UK's largest designated wetland [20,37]. It is a network of artificial lakes and rivers supporting 28 Sites of Specific Scientific Interest (SSSIs) and providing habitat for around a quarter of the UK's rarest flora and fauna species. These attributes produce approximately £568 million annually through tourism revenue [20,33]. The catchment's underlying geology consists predominantly of chalk and limestone bedrock overlain by glacial alluvium [33]. This configuration contributes to spatial variability in hydrological responses. The exposed bedrock promotes groundwater infiltration and peak flow mitigation, while alluvium-capped areas increase surface runoff and sensitivity to intense precipitation. The Broads system is strongly influenced by the tidal regime, with saline intrusion posing a threat to freshwater ecosystems by reducing food availability and increasing the risk of large-scale mortality amongst indigenous species [21]. The risk is amplified by sea level rise, which enables saline waters to penetrate farther inland, particularly during summer low-flow periods when reduced river discharge limits the system's natural flushing capacity. In addition, sea level rise directly increases flood risk, by raising baseline water levels and expanding inundation extents in this low-lying landscape [20].

The Broads system and the wider Broadland catchment have long been susceptible to flooding, with historical events such as the 1953 ‘Big Flood’ and the 2013/14 winter floods having severe local implications [12,38–41]. This region is recognised as highly sensitive to climate change, particularly due to sea-level rise and the intensification of hydrometeorological events [2,42,43]. It is further characterised by dynamic socio-economic change, with concentrated populations and ageing infrastructure in urban centres, coupled with high levels of social vulnerability in rural coastal towns. These intersecting physical and socio-economic characteristics make Broadland well suited to assessing climate-driven flood risk and the effectiveness of integrated risk methodologies.

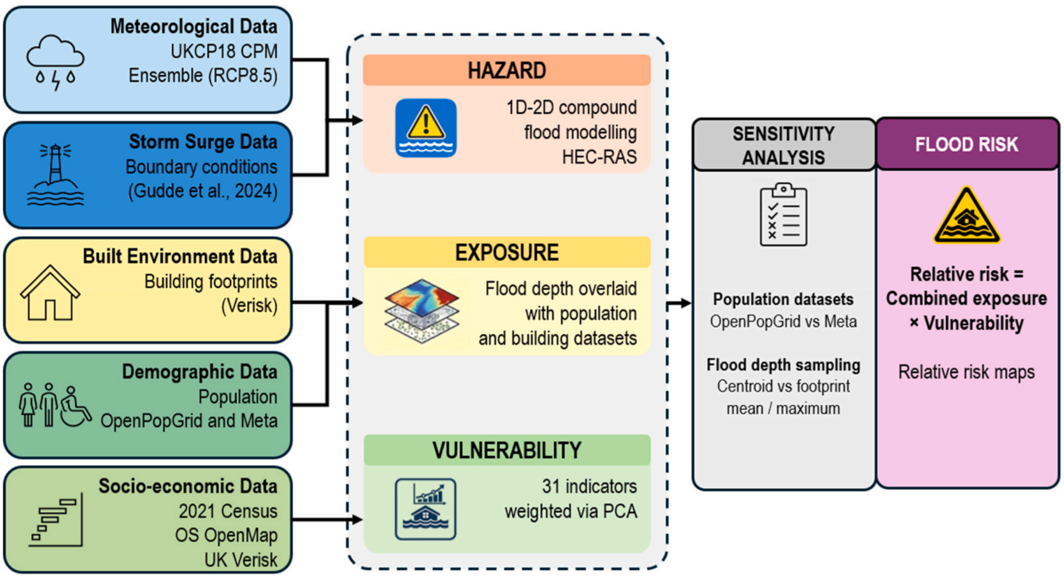

Fig. 1. Methodological workflow and input datasets used to derive hazard, exposure, vulnerability, and flood risk in the Broadland study area, including the sensitivity analyses undertaken. Hazard is represented through the scenario-specific inundation extent and depth used to derive exposure.

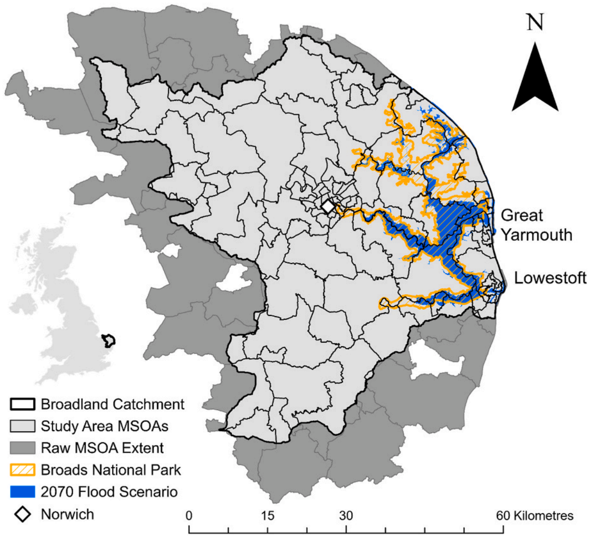

Fig. 2. The Broadland catchment, the Broads National Park and its Middle Super Output Areas (MSOAs). All MSOAs that intersect with the Broadland Catchment (the study area) are included in the study, with data collected from the full extent of each included MSOA (the dark grey area) not just that which intersects (the light grey area). The blue shading shows the modelled inundation extent from the 2070 compound-flood scenario from Gudde et al. [2].

2.2. Hydraulic model and flood scenarios

The HEC-RAS hydraulic model used to generate the inundation scenarios was originally developed and evaluated in Pasquier et al. [42] and subsequently refined and applied in Pasquier et al. [20] and Gudde et al. [2]. Model calibration and validation were undertaken using historical Environment Agency river-level observations. This study adopts the inundation rasters from Gudde et al. [2] as fixed hazard inputs.

This investigation examines three extreme inundation scenarios simulated in Gudde et al. [2], based on UKCP18 RCP8.5 local projections and tidal gauge data used to model river discharge and storm surge components, respectively. In Gudde et al. [2], the UKCP18 convection-permitting model (CPM) projections were used for three 20-year time slices, referred to by their midpoint years: 1990 (1981–2000), 2030 (2021–2040) and 2070 (2061–2080). The UKCP18 CPM ensemble is available only for RCP8.5 and equivalent CPM simulations were not produced for lower-emission pathways. Although both future periods are derived from RCP8.5, they do not represent the same degree of climate change. The 2030 time slice represents an earlier and comparatively less climate-affected state, whereas the 2070 time slice reflects a substantially stronger late-century climate signal under the same emissions pathway. The fluvial component varies across these scenarios through bias-corrected UKCP18 precipitation, temperature and derived evapotranspiration inputs used to drive the HBV-TYN hydrological model [44], from which 100-year return discharges were estimated. The coastal component varies through storm-surge boundary conditions adjusted using UKCP18 sea-level-rise projections, applied to a normalised Lowestoft surge profile. The simulations represent coastal and fluvial inundation only. Although climate-adjusted precipitation contributes to the derivation of river-discharge boundary conditions through the HBV-TYN hydrological model, rainfall was not applied directly to the land surface, and pluvial flooding caused by exceedance of infiltration or drainage capacity was not simulated.

Present-day defences are included (as of 2016), sourced from LiDAR data and built within the HEC-RAS modelling software [2,43]. Within this there was no consideration of defence failure, which in future study could be included along the lines of system risk analysis where defence performance is evaluated [45]. Each scenario combines a 100-year river discharge event and a 100-year coastal storm surge event. Assuming statistical independence between the two marginal events gives a nominal joint exceedance probability equivalent to a synthetic 10,000-year design event. This value should not be interpreted as a formally estimated joint return period for the Broadland catchment, because the dependence structure between river discharge and coastal surge was not modelled explicitly. The hydraulic model nevertheless represents the physical interaction of the imposed upstream and downstream boundary conditions, including tidal propagation and backwater effects. More rigorous estimation of compound-event probability would require a joint-probability or copula-based analysis of the fluvial and coastal drivers. This produced a synthetic 10,000-year compound flood, evaluated for three time periods. To isolate climate-driven changes in the modelled hazard, the population data, building exposure and vulnerability indicators were held constant across the three time periods. Present-day flood defences were also held constant. Defence failure, deterioration and future upgrades were not considered. This assumption reflects both data limitations and uncertainty in long-term projections of population and development patterns [46]. Risk was quantified at the MSOA level by integrating scenario-specific hazards with exposure and vulnerability indices for human and built environments.

2.3. Risk index

A scenario-based relative flood risk index was calculated for each MSOA. Hazard is represented by the scenario-specific inundation extent and flood depth from the compound-flood simulations. These hazard characteristics determine population exposure and built-environment exposure, including depth-related economic damage to buildings. Population exposure and building exposure were each rescaled to a 0–1 range and combined using equal weighting to derive the combined exposure index. The final risk index was then calculated as the product of the combined exposure index and the rescaled vulnerability index for MSOAs affected by the modelled inundation. Index values were ranked across the relevant MSOAs and classified into four quantile-based categories: low, moderate, high and very high. Hazard probability was not included as a separate multiplicative factor. The index therefore represents the relative spatial distribution of risk conditional on each fixed compound-flood scenario, rather than annual expected risk or probability-weighted loss. Although vulnerability was derived for the entire study area, only MSOAs with population or building exposure were included in the exposure and risk maps.

2.3.1. Exposure estimation and sensitivity analysis

Exposure was quantified separately for the population and the built environment. In this study, population exposure refers to the number of people located within areas exceeding the specified flood-depth threshold, while building exposure refers to inundated residential and non-residential properties and their associated direct economic losses. The term built environment is used to describe the physical building stock represented in the exposure analysis. In addition, sensitivity analyses were undertaken to assess how alternative population datasets, flood-depth thresholds, and building delineation methods influenced estimates of exposure and damage.

The relationship between flood depth and damage is well established for built assets, with numerous empirical and theoretical models linking inundation characteristics to property loss. In contrast, the relationship between flooding and impacts on people is more complex and cannot be represented using a simple depth-damage function [47–49]. Recent studies have proposed probabilistic approaches for assessing pedestrian instability or loss probability in floodwater, using information on flood characteristics such as water depth and flow velocity, together with assumptions about pedestrian vulnerability and stability [50,51]. These approaches provide a more detailed representation of risk to people, but their full application requires hydraulic and vulnerability information beyond the simplified exposure data used in the present study. Human exposure was therefore estimated using a simplified binary method, similar to that of Sayers et al. [18], where a spatial unit was considered exposed only if flood depths exceed a critical threshold. A flood-depth threshold of 0.5 m was adopted based on Ramsbottom et al. [52], Fg. 4.1) who identify this depth as the point at which hazard or damage begins to occur.

Human exposure was estimated using the flood extents generated from the HEC-RAS flood model overlaid with spatial population datasets. Two alternative gridded population datasets were used to explore the uncertainties in population mapping within flood risk assessment and to compare resulting exposure estimates and error metrics. The first was OpenPopGrid (OPG, [1]), which dasymetrically redistributes 2011 UK Census headcounts into 10 m grids using residential building polygons from Ordnance Survey (OS) vector layers. This dataset aligns well with the 2 m resolution HEC-RAS flood maps. The second was Meta's Humanitarian Data Exchange (HDX) population dataset (HDX, 2026) [53], produced in Meta's Data for Good project which uses machine learning, satellite imagery, and global navigation satellite system (GNSS) signal tracking to estimate global population distributions [54]. Available at 1 arc-second resolution (∼30 m resolution at the equator) in both GeoTIFF raster and CSV formats, the Meta dataset was used as an alternative gridded population product to the 10 m OpenPopGrid dataset.

Buildings can be represented by polygons of building footprints in datasets such as OS OpenMap and UKBuildings from Verisk. The open-source OS OpenMap datasets do not provide building-use attributes (e.g. residential, commercial and industrial), unlike premium OS products such as the National Geographic Database (NGD). Previous research has explored predicting residential and non-residential properties from standard OS layers using a machine-learning approach [55]. Such additional processing was considered beyond the scope of this study. A more complete source is the UKBuildings dataset from Verisk 3D Visual Intelligence UK, which provides building details including use, age, height and area. Furthermore, this dataset boasts greater disaggregation of building clusters, especially in dense urban areas. The Verisk dataset provides the spatial and attribute detail necessary for reliable exposure and damage estimation.

A sensitivity analysis was conducted to assess how different methods for defining exposed units affect estimates of exposure and damage, given the limited consistency in such definitions across the literature. Two delineation methods and three flood-depth measurements were tested following the guidance in Section 4 of Environment Agency [56]. The delineation methods were geometric building centroids and full building footprints. For the centroid-based method, a single flood-depth value was assigned to each building. For the footprint-based method, mean and maximum inundation depths within the building footprint were used. Because polygon-based data can lead to double counting along MSOA boundaries during aggregation, affected units and their associated flood depths were converted to centroids prior to aggregation.

The most common depth–damage functions linking flooding to property loss use a unit-loss approach, whereby damage per unit is derived from a maximum economic loss and an associated damage function [57,58]. A wide range of depth–damage function suites has been developed for estimating direct tangible damage in different regions. Multi-national and global repositories, such as those of Gerl et al. [59], Pregnolato and Galasso [60], and Bombelli et al. [61], illustrate the breadth of work in this field. In the UK, the Multi-Coloured Manual [48] is widely used and includes an extensive set of damage functions. However, its restricted accessibility makes it less suitable for transparent, open-access research. This study therefore used the European depth–damage dataset of Huizinga et al. [62], which provides open-source functions for broad occupancy classes compatible with the available UK building data. No local recalibration was undertaken. Although previous research has examined the transferability of flood-loss functions between regions [15], the applicability of the Huizinga et al. functions to local UK building stock remains a source of uncertainty.

The available building dataset did not include property-level characteristics known to influence flood damage, such as first-floor elevation, basement presence, number of storeys, construction materials or property-level flood-resistance measures. The resulting damage estimates therefore represent average occupancy-specific relationships rather than detailed predictions of structural vulnerability for individual buildings.

Because the detailed occupancy classes in the Verisk dataset did not correspond directly to the broader building classes used in the Huizinga et al. [62] depth–damage functions, a deterministic rule-based crosswalk was applied (Table S1). Municipal occupancies were mapped to the commercial class. Agricultural occupancies represented built structures rather than agricultural land or crop areas and were therefore mapped to the industrial building class. Where occupancy was recorded as unknown, no single class could be justified; these buildings were assigned the arithmetic mean of the residential, commercial and industrial depth–damage functions and corresponding maximum-damage values. These mappings represent methodological assumptions rather than the outputs of a statistically trained or independently validated building-classification model.

As the Verisk data included building footprint information, the damage per square metre values from Huizinga et al. [62] were applied. Final loss estimates were converted from EUR to GBP using historical exchange rates from Xe.com [63]. The 2010 GDP-based maximum damage values reported by Huizinga et al. [62] were adjusted to 2025 prices using the GDP deflators (28th March 2025) published by HM Treasury [63,64].

2.3.2. *Vulnerability estimation*

Vulnerability data were extracted from the full extent of all 107 MSOAs that intersect the Broadland hydrological catchment. Vulnerability was quantified through an end point multi-criteria approach, where pre-defined characteristics of the system, including those related to coping capacity, are identified and assigned, providing a positive or negative effect on vulnerability [65]. This approach provides a more holistic representation of vulnerability by accounting for longer-term effects of flooding. The derived vulnerability was assigned to the MSOA areas within the Broadland boundary for compatibility with the spatially bounded exposure data.

A total number of 56 base indicators were established through a literature review, reduced from an initially identified 67. These comprised social, economic and environmental indicators describing demographic sensitivity, socio-economic capacity, built-environment characteristics and environmental susceptibility. Data were primarily derived from the 2021 Census, OS OpenMap and the UK Verisk dataset, with demographic information mainly taken from the Census and spatial-environmental information derived from OS OpenMap and Verisk. All but three datasets were available at the MSOA level. Company size, housing value and income were available only at district level, so each district-level value was assigned to all MSOAs within the corresponding district [66]. Data sources and parent references are summarised in Tables S3 and S4.

Indicator suitability for principal components analysis (PCA) was subsequently assessed using the Kaiser–Meyer–Olkin (KMO) test, as described below. Table 1 provides a simplified summary of the indicator themes and examples used in the vulnerability assessment. The complete list of base indicators, including definitions, data sources, direction of effect and retained variables after KMO screening, is provided in Table S2.

Extraction and processing were performed using QGIS (spatial data) and R (demographic and further processing). Variables requiring normalisation were made proportional to their MSOA's total sample area or population. While studies such as Garbutt et al. [30] simplified indicators using a binary scoring system (0 = below the national average; 1 = above the national average), this study retained continuous indicator values to preserve spatial variability and better capture underlying patterns in the data.

Following the creation of the base index, the Kaiser-Meyer-Olkin test was applied using a threshold of >0.7, with inadequate variables omitted [67]. This test assesses the proportion of variance that may be attributed to common factors and is used to determine sampling adequacy. Bartlett's Test of Sphericity was then applied to assess whether the retained variables were sufficiently correlated for subsequent data reduction using principal components analysis [68]. A p-value of <0.01 was taken to indicate that it was appropriate to proceed with principal components analysis.

Principal components analysis (PCA) with varimax rotation was applied to reduce dataset dimensionality and intercorrelation among variables, and to derive loadings for the retained principal components (PCs). Although components with eigenvalues greater

Table 1
Simplified summary of vulnerability indicator themes used in the vulnerability assessment. The full list of base indicators, including definitions, data sources, direction of effect and retained variables after KMO screening, is provided in Table S2.

Theme	Indicator types included	Examples of indicators	Expected relationship with vulnerability
Social	Age, health, care needs, household structure, mobility, education	Age dependency ratio; population under 5; population over 65; persons in need of care; no vehicle access	Higher dependency, care needs and limited mobility generally increase vulnerability
Economic	Employment, economic diversity, education, housing/property characteristics, services and infrastructure	Economic diversity; educational diversity; workforce by sector; housing age; utility facilities; transport access	Greater diversity, resources and service access generally reduce vulnerability
Environmental	Elevation, erosion susceptibility, land use, urbanisation	Mean elevation; erosion-susceptible land; land-use diversity; urbanised area; unpopulated area	Lower elevation, erosion susceptibility and urbanisation generally increase vulnerability

than one are commonly retained in PCA [66], this criterion produced 16 PCs in the present study. A cumulative explained variance threshold of 80% was therefore adopted as a more pragmatic retention criterion, consistent with Saisana & Tarantola [69].

Prior to PCA, all variables were standardised using z-scores, with indicator direction defined according to whether higher values increased or reduced flood vulnerability. The varimax-rotated PCA outputs were used to derive a mean weighting for each of the 31 retained indicators. For the final index calculation, each retained indicator was rescaled independently to a 0–1 range. The rescaled value of each indicator was then multiplied by its corresponding mean PCA-derived weighting, and the weighted indicator values were summed to obtain the vulnerability score for each MSOA:

$$V_j = \sum_{i=1}^{31} w_i x_{ij}$$

where V_j is the vulnerability score for MSOA j, x_{ij} is the rescaled value of indicator i for MSOA j, and w_i is its corresponding mean PCA-derived weighting, with direction defined according to the positive or negative relationship shown in Table 2. The imported indicator weightings were applied directly, with no additional normalisation during the final aggregation stage. The resulting vulnerability scores were used to represent relative differences among MSOAs and were subsequently rescaled to a 0–1 range for integration with the exposure index.

3. Results

3.1. Exposure

This section presents exposure estimates alongside sensitivity analyses of population dataset choice, flood-depth thresholding and building-depth sampling method.

3.1.1. Population exposure

Despite similar total population estimates from the OpenPopGrid (OPG, 240,000) and Meta (242,000) datasets in the flood-affected region, estimated human exposure differs substantially between datasets. For the 1990 scenario, OPG yields 9071 exposed people

Table 2
Final indicators retained for the vulnerability index and their mean PCA-derived weightings. The sign shown for each indicator denotes whether higher indicator values increase (+) or reduce (−) vulnerability. In the final aggregation, each indicator was rescaled to 0–1, multiplied by its corresponding weighting and summed across all 31 indicators. The reported values are loading-derived coefficients and were not normalised to sum to 1.

Indicator (Effect) [Theme]	Mean weighting	Rank
Elevation (−) [Environmental]	0.020	1
Erosion (+) [Environmental]	0.017	2
Population under five (+) [Social]	0.014	3
Educational diversity (−) [Economic]	0.012	4
Student (−) [Social]	0.012	5
Land use diversity (−) [Environmental]	0.009	6
Age dependency (+) [Social]	0.009	7
Economic diversity (−) [Economic]	0.008	8
Utility facilities (−) [Economic]	0.008	9
Persons in need of care (+) [Social]	0.007	10
Hospitals (+) [Social]	0.007	11
Workforce in economic sectors (−) [Economic]	0.007	12
Single parent with dependent children (+) [Social]	0.007	13
No vehicle (+) [Economic]	0.007	14
Health centres (+) [Social]	0.007	15
Population density (+) [Social]	0.004	16
Commerce (−) [Economic]	0.004	17
Urbanised area (+) [Environmental]	0.004	18
Living space per person (−) [Social]	0.004	19
Population above 65 (+) [Social]	0.004	20
Median age (+) [Social]	0.002	21
Recovery (−) [Economic]	0.002	22
No secondary school diploma (+) [Economic]	0.002	23
Long term resident (−) [Social]	0.002	24
New resident (+) [Social]	0.002	25
Workforce in industry, construction and service sectors (−) [Economic]	0.002	26
Housing age (+) [Economic]	0.002	27
Transport (−) [Economic]	0.002	28
Residential buildings (+) [Economic]	0.002	29
Unpopulated area (−) [Environmental]	0.001	30
Central age (−) [Social]	0.001	31

while Meta yields 10,821 (≈19% higher), with enhanced differences in 2030 (OPG 9,184, Meta 11,126, ≈21% higher) and 2070 (OPG 12,308, Meta 15,461, ≈26% higher). OPG was selected as the best candidate for all following methodological steps due to its lower Root Mean Square Error (RMSE), calculated against 2021 Census population totals aggregated at MSOA level. OPG produced a lower RMSE than Meta across all locations (421.1 OPG versus 503.0 Meta) and in the most influential locations (top ten locations by population exposed; 379.1 OPG versus 721.7 Meta). This reflects larger discrepancies between Meta and the 2021 Census at the extremes, both in over- and under-representation.

Population exposure is primarily concentrated in Great Yarmouth, where several high-exposure MSOAs dominate the overall exposure totals (Fig. 3). Although these locations contain only 19.5% of the total OPG population, they account for 93% of the total exposure (1990 scenario). This relationship remains consistently significant although the dominance of these six Great Yarmouth locations reduces to 92% then 79% as the flood extents increase and inundate new areas. Reinforcing this are low median values, for example nine people exposed for OPG in the 1990 scenario, where the extremes of Great Yarmouth exposure mask a general lower magnitude of exposure elsewhere.

3.1.2. Building exposure

The sensitivity analysis between the three depth derivation methods (centroid, building footprint mean and maximum) yielded significant differences. Use of the building centroid produced the lowest total economic loss values across all scenarios. In the base scenario (1990), the centroid method produced £257 million of economic loss (Fig. 4). The footprint mean method was 22% greater at £312 million and the footprint-maximum was 71% above the centroid method at £439 million. Total event losses increased markedly, with the centroid totals increasing 16% (2030; £297 million) and 93% (2070; £495 million) relative to 1990. Similar relationships were shown for the footprint mean and maximum, both increasing 4% in 2030 relative to 1990 (£323 million and £457 million, mean and maximum respectively) and increasing 70% and 64% in 2070 relative to 1990 (£530 million and £718 million, mean and maximum respectively). Although losses increase across scenarios, the percentage difference relative to the centroid method decreases over time (from 22% in 1990, 9% in 2030, to 7% in 2070 for footprint mean, and from 71% in 1990, 54% in 2030, to 45% in 2070 for footprint-maximum). As flood extents and depths increase in the 2030 and 2070 scenarios, more buildings are inundated above damaging thresholds across their footprints, making exposure estimates less sensitive to whether depth is taken at the centroid or as the footprint mean/maximum.

For the headline risk estimates, we use the footprint-maximum depth as a conservative upper-bound assumption. This choice minimises the risk of underestimating damages for partially inundated buildings where local depth gradients occur within a footprint and provides a precautionary basis for adaptation planning. Centroid and footprint-mean methods are retained as lower-bound alternatives to characterise methodological uncertainty (Fig. 4). Using the footprint-maximum method, estimated exposure losses are £439 million (1990), £457 million (2030), and £718 million (2070), derived from 9,021, 9,309, and 12,705 exposed buildings, respectively.

Within the exposed MSOAs, the composition of the building inventory is dominated by residential (73%) and commercial (20%) occupancies. Although total economic losses increase across scenarios, the relative contribution of each occupancy class remains broadly consistent (Fig. 5). Commercial properties are the dominant driver of loss, accounting for approximately 51–53% of total losses across all scenarios (£228 million in 1990, £233 million in 2030 and £379 million in 2070). Residential buildings contribute 32–36% of losses despite representing a larger share of exposed properties (73–76%), reflecting their lower unit values. Industrial properties account for 8–10% of losses (£33 million in 1990, £36 million in 2030 and £71 million in 2070), exceeding their share of the building inventory, likely due to higher concentrations in areas exposed to tidal flooding around Great Yarmouth and Lowestoft. The remaining

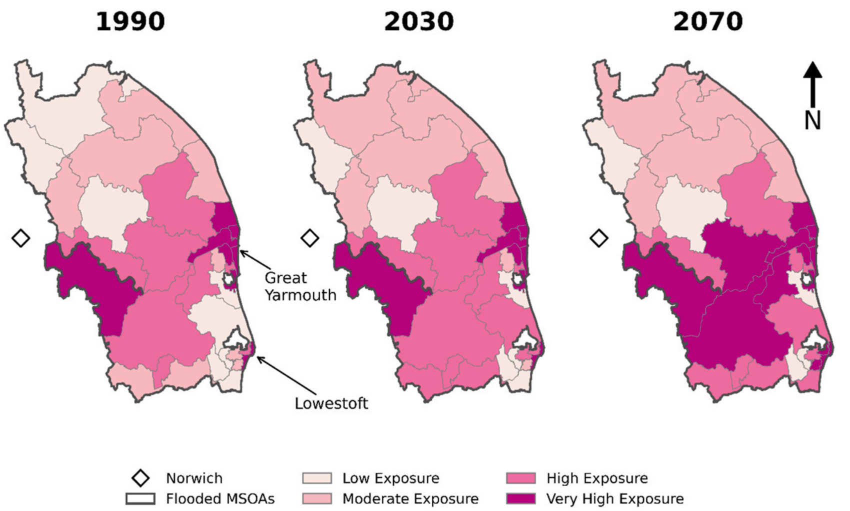

Fig. 3. Population exposure within the flood-affected MSOAs for each scenario. Values are classified into quartiles, ranging from low to very high population exposure.

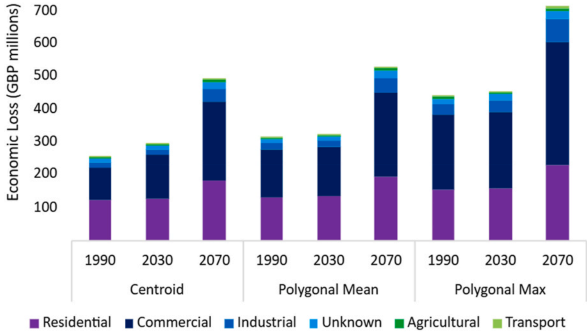

Fig. 4. Economic loss (GBP millions, present-day value) across all occupancies for the three depth-damage derivation methods (centroid, polygonal mean, and polygonal maximum). Agricultural and transport occupancies contribute only minor proportions of total loss and therefore appear only as small components of the stacked bars.

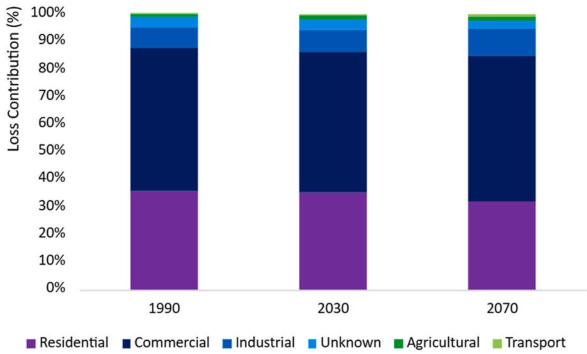

Fig. 5. Percentage contribution of economic losses by building occupancy class for the polygonal maximum depth–damage derivation method across the 1990, 2030 and 2070 scenarios.

occupancy classes contribute only small proportions of total losses, with unknown use accounting for 3–4%, agricultural 1.1–1.4%, and transport 0.1–1.0%.

The top ten loss-driving locations were Great Yarmouth (75% of total 1990 loss, with 45% of the total attributed to Great Yarmouth 007), Broadland 017 (containing a large industrial facility on the bank of the River Yare; 5.8%) and Lowestoft (6.1%) (Fig. 6). The three-digit codes refer to individual MSOAs. Representing 81% of all losses in the 1990 scenario, it is evident that the tidal-dominated,

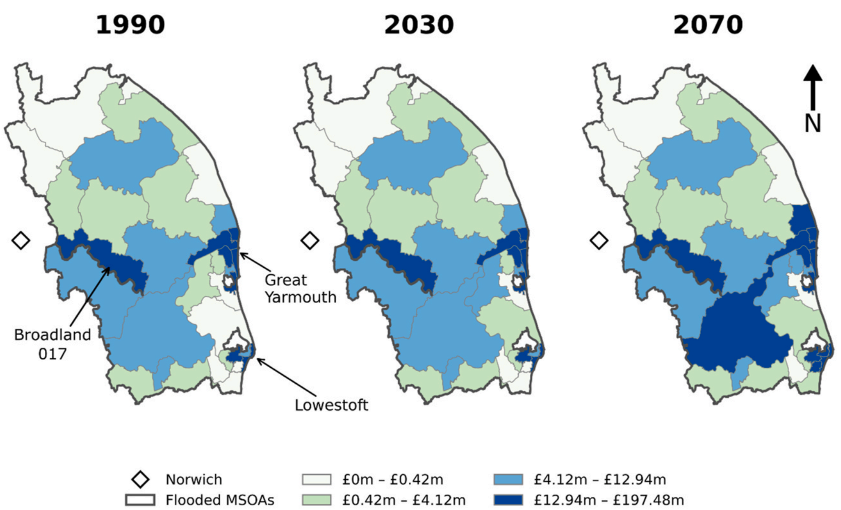

Fig. 6. Exposure of the built environment within the flood-affected MSOAs for the 1990, 2030 and 2070 scenarios. Values are economic damage in GBP millions indexed to present day and shown as quartiles.

urban centres of Great Yarmouth and Lowestoft are the dominant contributors to modelled economic losses. The lower median losses (£4.1 million in 1990, £4.5 million in 2030 and £8.3 million in 2070) indicate a skewed distribution in which a small number of urban coastal MSOAs (in Great Yarmouth and Lowestoft) contribute disproportionately to the total losses. The contribution of the top loss locations decreases in the 2030 and 2070 scenarios, where loss is spread further across the affected region.

Human and built exposure showed significant spatial correlation. However, there were some differences that underlie the final combined exposure distribution (Fig. 7). Human exposure was very concentrated, primarily in Great Yarmouth, leading to a handful of peripheral MSOAs in this area showing significant exposure throughout all scenarios. Built exposure showed slightly more variation, driving greater exposure in western Lowestoft. Scaled values for exposure can be found in Table S5.

3.2. Vulnerability

The Kaiser-Meyer-Olkin statistical test removed 25 variables below a score of 0.7, leaving 31 remaining indicators. The p-value for Bartlett's Test of Sphericity was $<2.22 \times 10\text{-}16$, far below the 0.01 threshold. Principal Components Analysis (PCA) determined eight principal components (PCs) with a cumulative proportion of variance explained of 81.2%. The first component explained 35.5% of the variance, with this proportion falling to 16.4% (PC2), then 8.16% (PC3) and 6.32% (PC4), with the remaining exhibiting progressively smaller proportions. The loadings of the varimax-rotated PCs identified 11 variable loadings of absolute values greater than 0.1, with maximums seen for workforce in industry, construction and service sector (0.451), new resident (0.425) and central age (−0.385). The resultant statistically assigned weightings from the PCA analysis (Table 2) range from 0.020 (Elevation) to 0.001 (Central age).

Vulnerability showed clear correlation with coastal and urban regions (Fig. 8). This is driven by environmental factors with lower elevations and lower land use diversity as well as social factors with higher population below five and lower educational diversity. Further impact is shown in urban regions from low economic diversity while some more rural, coastal regions showed influence from higher erodibility. Standardised total vulnerability ranges from −0.010 to 0.037 with a median of 0.01. Great Yarmouth 011 (Fig. 8) was the most vulnerable at 0.037, driven significantly by low rankings in indicators with heavily negative weightings (elevation, educational diversity and land use diversity at 78th, 98th and 107th, out of 107 locations respectively) and high rankings in the significantly positive weighted population below five (10th). Great Yarmouth 007 and 009 (Fig. 8) display similar characteristics (vulnerability of 0.036 and 0.034, respectively), with low rankings in strong negative weighted indicators of elevation (106th and 84th, respectively), educational diversity (106th and 103rd, respectively) as well as land use diversity for 009 (76th), while ranking highly in the influential positively-weighted population below five indicator (3rd and 9th, respectively).

Conversely, Norwich 017, Broadland 002 and Breckland 010 (Fig. 8) were the three least vulnerable locations at vulnerability values of −0.01, −0.0087 and −0.0083, respectively. Despite a low ranking of 72nd in the negatively-weighted elevation indicator, Norwich 017 held significantly low rankings for the positively-weighted erosion, population below five and age dependency indicators (72nd, 92nd and 107th) in addition to high rankings in the negatively-weighted educational diversity and student indicators (3rd and 2nd). Broadland 002 and Breckland 010 (a location with minimal intersection with the study area) ranked moderately high in elevation (28th and 22nd) and low in population below five for the former (80th) and erosion for the latter (85th). The effects of this were enhanced in the aggregate by moderately low rankings in positively weighted indicators and moderately high rankings in negatively weighted indicators. Scaled values for vulnerability in flood-exposed MSOAs are found in Table S5.

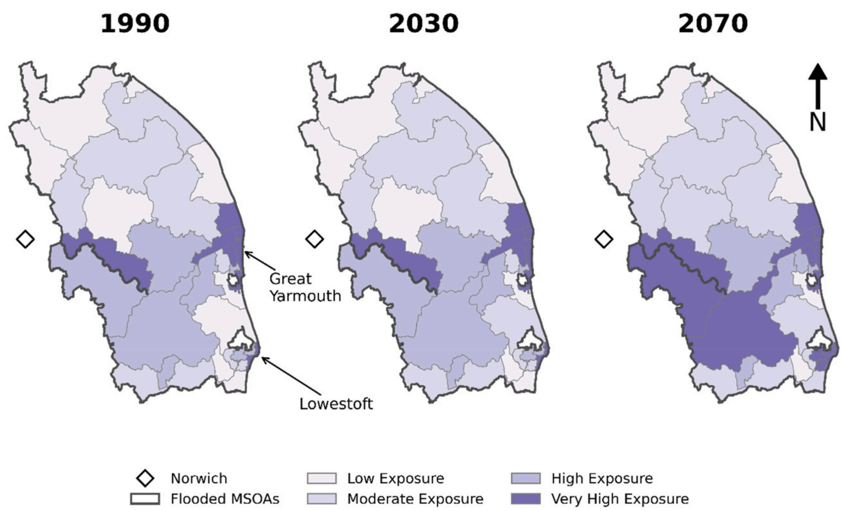

Fig. 7. Combined exposure of the human and built environment within the flood-affected MSOAs for the 1990, 2030 and 2070 scenarios. Values are classified into quartiles, ranging from low to very high combined exposure.

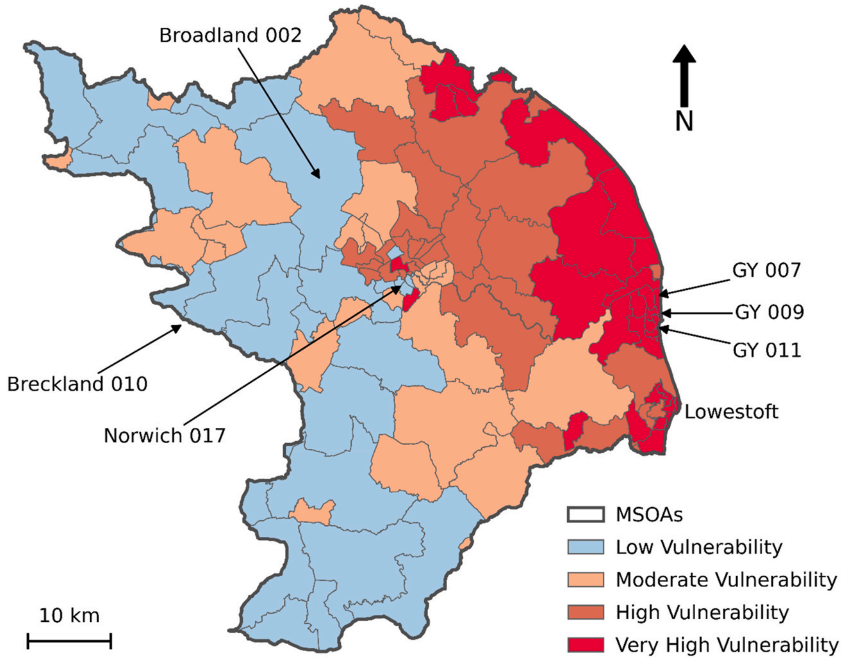

Fig. 8. Vulnerability within the MSOAs. Colour scale shows quartiles as low vulnerability (blue) to very high vulnerability (red). Label "GY" represents "Great Yarmouth". Three-digit codes refer to MSOAs.

3.3. Risk

Driven by consistently high exposure and elevated vulnerability, the urban and coastal towns of Great Yarmouth and Lowestoft exhibited the greatest magnitudes of risk across all scenarios (Fig. 9). While it was observed that the most vulnerable region, Great Yarmouth 011, was not included in the final locations at risk due to not experiencing any inundation, dominance was shown by Great Yarmouth 007, 005 and 006 which remained first, second, and third from 1990 to 2070. 1990 and 2030 showed similarity, where the relatively modest increase in exposure produced minimal variation, before significant change occurred from 2030 to 2070. The largest variation from 2030 to 2070 was exhibited in Lowestoft where East Suffolk 006 moved from 7th to 4th and East Suffolk 009 moved even further from 21st to 8th. Lowest risk was observed in more expansive rural regions where the density (and consequently exposure) of the human and built environment are lower, with additional vulnerability mitigation due to higher elevation further inland. Scaled values for risk in flood-exposed MSOAs are found in Table S5.

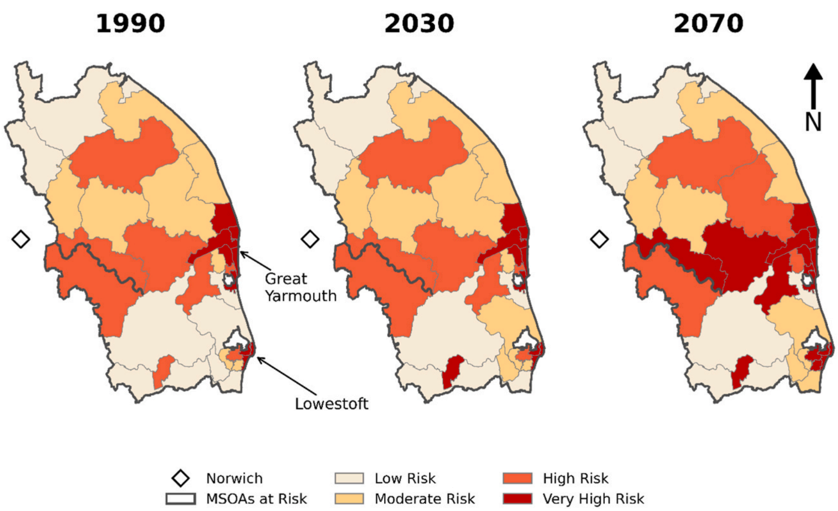

Fig. 9. Scenario-based relative flood risk within the flood-affected MSOAs for each scenario. Values are classified into quartiles, ranging from low to very high relative risk.

4. Discussion

4.1. Exposure estimates and methodological sensitivity

Compared with other studies within the domain, greater exposure was generally observed (combined totals for residential, industrial and commercial buildings of 9,021, 9309 and 12,705 for the 1990, 2030 and 2070 scenarios respectively) with Pasquier [43] detailing property exposures of 3579 (2030 scenario) and 4109-4945 (2055-2080 scenarios). These differences likely reflect the methodological choices in exposure delineation. The use of 'binary exposure' [18] increases the sensitivity of the exposure derivation process, where any small changes in flood extent can cause intersection and subsequent 'exposure' of further properties. Such methods are more useful as a precautionary tool to establish all elements with potential for any level of damage. This method can select above a 'critical threshold', where elements that are predicted to experience inundation above this water depth are considered exposed [70]. The most comprehensive method uses depth-damage functions to establish total damage or loss across a region, where elements are aggregated across fractions of a depth-damage function, with these fractions being associated with an economic loss [71]. Shepard et al. [29] is a classic example of these methods, where population exposure is assessed via critical threshold and property exposure employs depth-damage functions from the Federal Emergency Management Agency's (FEMA) Hazus-MH Flood Model software. Equivalence was found in a more manual process using vulnerability curves from Huizinga et al. [62] and ArcGIS. This manual process promotes complete flexibility in damage derivation; however, quality assurance checks must be implemented thoroughly.

Furthermore, it is important to assess the sensitivity of the results to key methodological steps and ensure the chosen assumptions remain conceptually robust. This study shows that apparently minor choices can introduce substantial uncertainty: in the 1990 scenario, estimated building exposure losses increase from £257 million (centroid) to £439 million (footprint-maximum), a 71% difference. While this choice of property representation is often constrained by data availability, decisions should be made based on how the underlying depth-damage functions are defined and applied. In practice, property-level impact estimation commonly relies on simplified representations of flood depth at the building scale, and guidance for local flood risk assessment explicitly notes that extracting depth at a point (property locations) versus across a building footprint—and selecting mean versus maximum depth within that footprint—may have significant implications for the depths returned [56]. Footprint-maximum sampling can be viewed as a conservative representation where depth varies strongly within a footprint, but it may overestimate damages if only a small part of the building is affected. Conversely, centroid (point) sampling is computationally efficient and avoids applying a single extreme depth across a footprint but may underestimate damages where depth variability within a building footprint is substantial [56].

In addition to uncertainty associated with depth sampling and the transferability of the depth–damage functions, property-level characteristics that can substantially influence observed damage—including first-floor elevation, basement presence, number of storeys, construction materials and flood-resistance measures—were not consistently available. The estimated losses should therefore be interpreted as aggregate screening estimates rather than predictions for individual buildings. Their primary value lies in comparing scenarios and identifying spatial concentrations of potential damage that may warrant more detailed appraisal.

The sensitivity of estimated losses to building-depth sampling is consistent with the wider literature showing that flood-risk estimates depend on model structure, datasets and analytical assumptions. The contribution here is to quantify the magnitude of this effect within a high-resolution compound coastal–fluvial assessment. For decision support, the alternative estimates may be interpreted as a methodological range rather than as competing predictions from which a single value must be selected. This can help distinguish conclusions that remain stable across assumptions from those that are more assumption-dependent. Such an interpretation is consistent with decision-making under deep uncertainty, which emphasises strategies that perform acceptably across multiple plausible futures rather than optimisation for a single assumed future [72–74].

While more discriminative selection, such as binary exposure, may not capture the full spatial variability of inundation within buildings, population exposure often requires thresholding because there is no widely accepted depth–damage relationship for human harm. Therefore, critical thresholds must be applied, with this study setting this limit at 0.5 m based upon the initiation depth of harm to humans in Ramsbottom et al. [52], Fg. 4.1). However, the choice of threshold can substantially affect estimated exposure. For methodological comparison, Sayers et al. [18] and Gudde et al. [2] define exposure as any inundation, corresponding to a 0 m threshold, whereas the present study applies a 0.5 m threshold to represent the onset of potential harm to people. On the same OPG data and same compound flood scenarios, Gudde et al. [2] report exposure counts of 13,917 (1990), 14,088 (2030) and 18,785 (2070) which are approximately 53% higher than the 0.5 m threshold exposure counts used in this study. This comparison demonstrates that population exposure estimates are sensitive to threshold choice, even where the same population dataset and flood scenarios are used. For broader context, the Broadland Rivers Catchment Flood Management Plan (CFMP, [33]) reports that at present around 3900 people are at risk within the CFMP area, noting that risk arises from river flooding (1% annual probability), tidal flooding (0.5% annual probability) and, in some locations, a combination of both. The same report provides future (2100) people-at-risk estimates for the Great Yarmouth and Lowestoft sub-areas (10,309 and 4,051, respectively), highlighting the potential for substantially increased exposure over the long term [33]. The CFMP estimates are not directly comparable with the threshold-based exposure estimates used here because they are based on Environment Agency flood-risk mapping assumptions rather than a gridded depth-threshold overlay.

The projected increase in property and population exposure is consistent with wider UK evidence. Under a 2°C warming pathway by 2100 and excluding coastal erosion, annual flood losses for non-residential properties are projected to increase by 27% by 2050 and 40% by 2080 [18,75]. Similarly, the exposed population is projected to increase from 2 million (2018) to 6.4 million (by the 2080s) in a 4°C future with current adaptation [13]. However, long-term exposure trajectories remain highly uncertain because socio-economic pathways (e.g., demographic change, development patterns, and future adaptation) are too diverse to assess with traditional methods [76]. Observed trends nevertheless indicate substantial development in UK floodplains [77]. Continued floodplain development would increase the number of assets and people located in high-hazard areas and could also alter flood dynamics through changes in floodplain conveyance and land cover [78].

Methodological choices also introduce uncertainty, particularly the selection of datasets used to represent population distribution. With OpenPopGrid [1] and Meta [54] being directly compared, we found OpenPopGrid to be more representative within this study area when compared against the 2021 UK Census. This is likely due to OpenPopGrid disaggregating data directly from the 2011 UK Census [1]. Despite OpenPopGrid outperforming Meta, Meta's errors were concentrated in the highest-exposure (primarily urban) MSOAs, resulting in a higher RMSE for the top ten locations despite lower errors in some other areas. Given that Meta was designed to improve population mapping in data-sparse and rural settings [54,79], this pattern may reflect differing strengths of the two products across settlement types.

Overall, these results demonstrate that methodological choices in exposure delineation, population mapping and building-depth sampling can substantially affect estimated impacts, and therefore shape how flood-risk information is interpreted for adaptation planning.

4.2. Vulnerability

The spatial distribution of flood vulnerability shows higher values near urban centres (Fig. 8), with higher values exhibited near and within Great Yarmouth and Lowestoft. Conversely, lower vulnerability was observed in less densely populated MSOAs occupying larger extents in more rural and inland locations. Some intra-urban variation is evident in Norwich, where higher vulnerability in some MSOAs is associated with a higher proportion of children under five and greater erosion-susceptible land cover. This spatial trend generally agrees with a previous study on vulnerability in Norfolk by Garbutt et al. [30]. However, the most discernible difference is the area directly to the east of Norwich which Garbutt et al. [30] classifies as low vulnerability, while this study finds it to be high vulnerability. This heightened vulnerability is driven by a combination of factors: low-to-moderate elevation, high erosion susceptibility and high-to-moderate population below five.

The created vulnerability index provides a multi-dimensional representation of vulnerability by combining indicators across social, economic and environmental themes. The final index comprises 14 social, 12 economic and 5 environmental indicators (Table 2), distilled from an original set of 56 (Table 1). The inclusion of environmental indicators distinguishes this study from Shepard et al. [29], which only considered socio-economic dimensions of the affected system. In our study, elevation and erosion susceptibility are the two most highly weighted indicators (0.020 and 0.017, respectively). The retained indicators span social, economic and environmental themes, but the two highest individual PCA-derived weights were assigned to the environmental indicators elevation and erosion susceptibility. This indicates a comparatively strong influence of environmental characteristics on the index, although indicators from all three themes contributed to the final vulnerability pattern. This reinforces the analysis of the application of weightings conducted within Kotzee & Reyers [32], who highlight the value of PCA-based weighting in capturing multi-dimensional socio-ecological interactions. Additionally, PCA reduced the dimensionality of the dataset while retaining a comprehensive index of indicators with sufficient sampling adequacy [69,80,81]. Alternative approaches, including stakeholder-led or expert-based weighting, may better reflect decision priorities but introduce their own subjectivities regarding stakeholder selection and preference reconciliation [81,82]. Similarly, there is contention on indicator selection, where subjectivity or reliance on specific conceptual models could create bias [83]. In this study, we sought to reduce such subjectivity by drawing indicators broadly from the literature, followed by statistical screening for redundancy and multicollinearity and PCA-based weighting [84]. Nevertheless, some bias is unavoidable because any operational definition of vulnerability shapes indicator selection and interpretation.

Alternative unsupervised approaches, including clustering, self-organising maps and nonlinear representation-learning methods, could potentially identify vulnerability structures or interactions not captured by linear PCA [85]. However, such methods would not remove the underlying constraints associated with indicator availability, spatial aggregation and the relatively small sample of 107 MSOAs, and their outputs would require careful evaluation for stability and interpretability. Future work could compare PCA-derived indices with alternative unsupervised approaches where larger spatial samples and independent validation data are available.

Constructing the vulnerability index at LSOA or Output Area level could reveal finer intra-MSOA differences and improve spatial alignment with the hazard and exposure components. However, fewer indicators are consistently available at these scales, and the use of smaller spatial units may increase sensitivity to small denominators, disclosure controls and unstable rates. The selected MSOA scale therefore represents a compromise between spatial detail, indicator completeness and statistical robustness.

4.3. Risk

The combined exposure index and vulnerability index were multiplied to derive the scenario-based relative flood risk. Because vulnerability is assumed stationary across time periods, changes in risk between 1990, 2030, and 2070 are driven primarily by changes in hazard extent and associated exposure. This assumption is necessary given the limited availability and high uncertainty of long-term projections for socio-economic vulnerability at MSOA scale. In principle, temporally varying vulnerability could be explored through projected changes in population [18] and the built environment (i.e. property density) [28,86], but they are highly uncertain and scenario dependent. The spatial pattern of risk illustrates the value of interpreting hazard, exposure and vulnerability together. Locations such as Great Yarmouth and Lowestoft emerge as persistent hotspots because high exposure coincides with elevated vulnerability within the modelled inundation extent. Conversely, the example of Great Yarmouth 011, which has the highest vulnerability score but is not included in the final risk locations because it is not inundated under the simulated scenarios, shows that vulnerability alone does not determine flood risk. This distinction is important for adaptation planning because it helps differentiate locations where vulnerability coincides with modelled flood exposure from those where vulnerability is high but hazard exposure is limited under the scenarios assessed.

Physical building damage and human vulnerability are represented as analytically distinct dimensions in this framework, but they are not independent in practice. Building damage can contribute to displacement, disruption of services, adverse health and wellbeing outcomes, and reduced recovery capacity. Conversely, socio-economic conditions can influence housing quality, preparedness, insurance access and the ability to repair or adapt properties. The present framework combines the spatial patterns of these dimensions at MSOA level but does not explicitly model causal, feedback or nonlinear interactions between them. Treating them separately preserves transparency between direct tangible losses and area-level social vulnerability and avoids imposing an interaction structure that cannot be supported by the available data, but it may underrepresent locations where physical and social disadvantages reinforce one another.

A further consideration is the transferability of the methodology to other study locations. The conceptual structure of the framework—integrating hazard, exposure and vulnerability—is transferable across coastal and estuarine settings, but the specific datasets, spatial units and parameterisations used here are context dependent. The approach is therefore most readily applied in data-rich settings where census information, building footprints, land-cover indicators and suitable flood-damage relationships are available at compatible spatial resolutions [87]. In other settings, the Verisk building inventory, UK census indicators and MSOA geography would need to be replaced with locally appropriate data, while depth–damage functions may require local calibration or validation.

In data-poor regions, global building exposure products [88,89] and gridded population datasets [54,90–92] may provide surrogate inputs. However, such substitutions are likely to reduce spatial detail and increase uncertainty, particularly in building occupancy classification, vulnerability characterisation and damage estimation. The framework should therefore be regarded as methodologically transferable rather than directly portable without local adaptation.

4.4. Implications for adaptation planning

The analysis does not evaluate individual adaptation measures, but it identifies where different forms of intervention may warrant further appraisal. MSOAs in which high exposure and high vulnerability coincide, particularly in and around Great Yarmouth and Lowestoft, may represent priorities for more detailed assessment of flood-defence investment, property-level resilience, emergency planning and targeted support for vulnerable populations. Areas where projected exposure increases markedly between scenarios may also require closer consideration in land-use planning and development control.

The separate treatment of population exposure, building losses and vulnerability can help distinguish different adaptation needs. Locations dominated by high building losses may justify appraisal of structural protection or property-level measures, whereas areas with comparatively high social vulnerability may require strengthened warning, evacuation and recovery support. The results should be interpreted as a screening and prioritisation tool rather than as an evaluation of the effectiveness or cost-benefit performance of specific adaptation options. Selection among measures such as hold-the-line, managed realignment or property-level resilience would require additional modelling of intervention performance, costs, residual risk and stakeholder preferences (e.g. Ref. [93]). The scenarios used here are best interpreted as high-end stress tests rather than predictions of the most likely future. Their value for adaptation planning lies in identifying locations and risk components that may become critical under severe compound flooding. They can therefore support screening, contingency planning and prioritisation of locations for more detailed appraisal, but should be considered alongside more frequent events, alternative climate pathways (e.g. Ref. [94]) and intervention-specific analyses before major investment decisions are made.

4.5. Assumptions and limitations

The primary limitation of this study is the spatial extent of the hydraulic model domain, which captures the Broads and adjacent low-lying coastal areas but not the full Broadland catchment. The resulting risk estimates should therefore be interpreted as applying only to the modelled floodplain and not to the wider catchment. This focus was considered appropriate for the compound fluvial–tidal hazard examined here, for which storm surge impacts are expected to be greatest in and around Great Yarmouth and Lowestoft. An additional element of the hazard not represented here is pluvial (surface-water) flooding, which can be important in urban areas and is increasingly being assessed using high-resolution urban flood risk frameworks [95]. The reported exposure, damage and risk estimates relate specifically to the coastal–fluvial inundation scenarios modelled by Gudde et al. [2] and should not be interpreted as an assessment of total flood risk from all potential sources.

A key data limitation was the lack of dasymetric population distribution based on the 2021 UK Census. The OpenPopGrid distribution used here is based on the 2011 Census. Furthermore, we assume that the spatial distributions of the built environment and population remain stationary across the 1990, 2030, and 2070 scenarios. This assumption isolates climate-driven changes in hazard but may underestimate future exposure where floodplain development and demographic change increase the number of assets and people located in inundation-prone areas.

The assumption of stationary population, building stock and vulnerability isolates climate-driven changes in the modelled compound hazard, but is likely to underestimate future risk where population growth, floodplain development or increasing socio-economic disadvantage occur within inundation-prone areas. As an illustrative population-only bound, applying the 45% increase in floodplain population projected by Sayers et al. [13] uniformly to the modelled 2070 exposed population would increase the estimated number of exposed people from 12,308 to approximately 17,847. This represents around 5539 additional exposed people. However, this simple scaling does not account for the spatial distribution of population growth, changes in floodplain development, future adaptation or changes in vulnerability, and should therefore not be interpreted as a formal future exposure scenario. Likewise, the projected increase in deprived neighbourhoods cannot be translated directly into a proportional increase in the vulnerability index, because vulnerability is derived from multiple social, economic and environmental indicators whose future trajectories are uncertain.

Although MSOAs provided the finest common spatial unit across the full vulnerability indicator suite, aggregation at this scale may obscure intra-MSOA variation in vulnerability, particularly in heterogeneous urban areas. The resulting risk patterns should therefore be interpreted at MSOA scale rather than as neighbourhood- or property-level estimates.

A key assumption in the exposure methodology concerns building occupancy classifications, because the depth-damage functions are defined only for broad categories. Additional assumptions were required to map Verisk occupancy types to these classes, for example, assigning agricultural buildings to the industrial class and applying an average of residential, commercial, and industrial functions to buildings with unknown occupancy. Further work could benefit from sensitivity analysis to assess the effects of using different functions for these unrepresented occupancies. A further assumption is that the Huizinga et al. [62] damage functions are transferable to the study area. No UK-specific or local recalibration was undertaken. Although these functions provide transparent and open-access relationships for broad occupancy classes and have previously been applied in European and UK contexts, they may not fully represent local building construction, basement prevalence, property-level resilience measures or contents values. This introduces uncertainty into the absolute damage estimates. Future work could compare results across alternative UK and European function libraries and benchmark them against local post-event damage observations where available.

The depth–damage functions include direct tangible damages but not indirect damages such as business interruption or wider economic disruption, which can contribute substantially to total flood losses [96], or intangible impacts such as health and trauma. These omissions may lead to underestimation of total losses, but appropriate uplift factors are context dependent and remain uncertain.

A further limitation is how flood characteristics are translated into impacts for both buildings and people. For buildings, the hazard includes a substantial component of storm surge. Floodwater velocity, which is not included in the present damage estimation, may contribute additional property damage, particularly where high velocities occur near flow constrictions or defences are overtopped [97,98]. The magnitude of this effect could not be quantified because the applied depth–damage functions use inundation depth alone and locally applicable depth–velocity damage functions were unavailable. Consequently, the reported losses may underestimate damage locally where hydrodynamic forces are important. Conversely, site-level resistance measures (e.g., property-level protection) may reduce realised damages but are not represented here. For people, the relationship between flood characteristics and harm is more complex than for buildings. Although this study uses a depth threshold to estimate human exposure, risks to people may also depend on velocity, depth–velocity combinations, warning time, mobility, behaviour and local evacuation conditions [50–52,99]. The omission of velocity may therefore underestimate risk in areas where shallow but fast flows occur. Future work should apply velocity-informed or probabilistic approaches where suitable hydraulic outputs and exposure information are available.

Further work should test the robustness of the vulnerability index to alternative weighting schemes, indicator selections and spatial aggregation units, and should explore additional climate and socio-economic scenarios where suitable data are available. These extensions would help clarify how far the identified risk patterns depend on PCA-based weighting, MSOA-level aggregation and the assumption of stationary exposure and vulnerability.

A final assumption relates to the inflation and currency adjustments used to express all losses in present-day monetary terms. Alternative choices, such as valuing each scenario in its corresponding year, could affect the comparability of monetary losses across time slices.

5. Conclusions

This study applied an integrated flood risk assessment framework to evaluate climate-driven compound flood risk in Broadland, with particular emphasis on how methodological choices influence exposure, damage and spatial risk estimates. We show that outcomes can be highly sensitive to methodological choices that may appear to be minor. For example, how flood depth is sampled for buildings or how exposure is delineated can substantially influence estimated losses. The results highlight strongly skewed risk patterns, with disproportionate exposure and risk concentrated in coastal urban areas, particularly Great Yarmouth and Lowestoft. These spatial patterns can support the prioritisation of locations for more detailed appraisal of flood-defence investment, property-level resilience, emergency planning and land-use controls. However, the study does not evaluate the effectiveness or cost-benefit performance of specific adaptation options. Elevated risk is also identified within parts of the Broads National Park floodplain, where development overlaps with areas susceptible to surge-related inundation. Under the assumption of stationary vulnerability, changes in risk across scenarios are driven primarily by changes in hazard and resulting exposure. Using the footprint-maximum depth method for building impacts, estimated exposure losses increase from £439 million (1990) to £457 million (2030) and £718 million (2070).

Further work should test the robustness of the vulnerability index to alternative weighting schemes, indicator selections and spatial aggregation units, and should explore additional climate and socio-economic scenarios where suitable data are available. These extensions would help clarify how far the identified risk patterns depend on PCA-based weighting, MSOA-level aggregation and the assumption of stationary exposure and vulnerability. A formal decision-making-under-deep-uncertainty assessment would additionally require testing alternative adaptation options against explicit performance criteria across these plausible futures.

CRediT authorship contribution statement

Ross Gudde: Writing – review & editing, Writing – original draft, Methodology, Investigation, Formal analysis, Data curation, Conceptualization. **Yi He:** Writing – review & editing, Supervision, Resources, Methodology, Conceptualization. **Ulysse Pasquier:** Writing – review & editing, Methodology. **Paul B. Sayers:** Writing – review & editing.

Funding

This research was supported by the Open CLimate IMpacts modelling framework (OpenCLIM) project funded by the UK Natural Environment Research Council award number NE/T013931/1. Development of the paper has been supported by the Open Evaluation of Climate-Resilient Interventions for Land Management, Soil Health and Net Zero (OpenLAND) project funded by the UK Biotechnology and Biological Sciences Research Council, award number BB/Z516168/1.

Declaration of competing interests

The authors declare the following financial interests/personal relationships which may be considered as potential competing interests: Yi He reports financial support was provided by UK Research and Innovation Natural Environment Research Council. Yi He reports financial support was provided by UK Research and Innovation Biotechnology and Biological Sciences Research Council. If there are other authors, they declare that they have no known competing financial interests or personal relationships that could have appeared to influence the work reported in this paper.

Appendix A. Supplementary data

Supplementary data to this article can be found online at https://doi.org/10.1016/j.ijdrr.2026.106410.

Data availability

The exposure datasets are available from: OpenPopGrid [1]; Meta's Humanitarian Data Exchange (HDX) population dataset (HDX, 2026); OS OpenMap (EDINA Digimap); and Verisk UKBuildings (EDINA Digimap). The vulnerability datasets are available as detailed in Table S3 in the Supplementary Information document. Flood scenario rasters from Gudde et al. [2] are available from: https://doi.org/10.5281/zenodo.19510451.

References

[1] A.P. Murdock, A.J.P. Harfoot, D. Martin, S. Cockings, C. Hill, OpenPopGrid: an open gridded population dataset for England and Wales. GeoData, University of Southampton, 2015. Available at: https://openpopgrid.geodata.soton.ac.uk/.
[2] R. Gudde, Y. He, U. Pasquier, N. Forstenhäusler, C. Noble, Zha Qianyu, Quantifying future changes of flood hazards within the Broadland catchment in the UK, Nat. Hazards 120 (2024), https://doi.org/10.1007/s11069-024-06590-5.
[3] P.B. Sayers, J.W. Hall, I.C. Meadowcroft, Towards risk-based flood hazard management in the UK, Proc. Inst. Civ. Eng. Civ. Eng. 150 (5) (2002) 36–42, https://doi.org/10.1680/cien.2002.150.5.36.
[4] M. Leonard, S. Westra, A. Phatak, M. Lambert, B. van den Hurk, K. McInnes, J. Risbey, S. Schuster, D. Jakob, M. Stafford-Smith, A compound event framework for understanding extreme impacts, Wiley Interdiscip. Rev. Clim. Change 5 (1) (2013) 113–128, https://doi.org/10.1002/wcc.252.
[5] D. Crichton, The risk triangle, in: J. Ingleton (Ed.), Natural Disaster Management. London: Tudor Rose, 1999, pp. 102–103.
[6] Y. He, F. Pappenberger, D. Manful, H. Cloke, P.D. Bates, F. Wetterhall, B.L. Parkes, Flood inundation dynamics and socioeconomic vulnerability under environmental change, Flood Risk Management in Europe (2013) 241–255, https://doi.org/10.1016/b978-0-12-384703-4.00508-6.
[7] B. Merz, A.H. Thieken, M. Gocht, Flood risk mapping at the local Scale: Concepts and challenges, Flood Risk Management in Europe (2007) 231–251, https://doi.org/10.1007/978-1-4020-4200-3_13.
[8] O.D. Cardona, M.K. van Aalst, J. Birkmann, M. Fordham, G. McGregor, R. Perez, R.S. Pulwarty, E.L.F. Schipper, B.T. Sinh, H. Décamps, M. Keim, I. Davis, K. L. Ebi, A. Lavell, R. Mechler, V. Murray, M. Pelling, J. Pohl, A.-O. Smith, F. Thomalla, Determinants of risk: exposure and vulnerability, Managing the Risks of Extreme Events and Disasters to Advance Climate Change Adaptation (2012) 65–108, https://doi.org/10.1017/cbo9781139177245.005.
[9] R.D. Kusumastuti, Viverita, Z.A. Husodo, L. Suardi, D.N. Danarsari, Developing a resilience index towards natural disasters in Indonesia, Int. J. Disaster Risk Reduct. 10 (2014) 327–340, https://doi.org/10.1016/j.ijdrr.2014.10.007.
[10] P.J. Baxter, The east coast Big Flood, 31 January–1 February 1953: a summary of the human disaster, Philos. Trans. R. Soc. A Math. Phys. Eng. Sci. 363 (1831) (2005) 1293–1312, https://doi.org/10.1098/rsta.2005.1569.
[11] Cabinet Office, National Risk Register of Civil Emergencies, Cabinet Office, London, 2010.
[12] T. Spencer, S.M. Brooks, I. Möller, Storm-surge impact depends on setting, Nature 505 (7481) (2014), https://doi.org/10.1038/505026b, 26–26.
[13] P. Sayers, E.C. Penning-Rowsell, M. Horritt, Flood vulnerability, risk, and social disadvantage: current and Future Patterns in the UK, Reg. Environ. Change 18 (2) (2018) 339–352, https://doi.org/10.1007/s10113-017-1252-z.
[14] F. Elmer, J. Hoymann, D. Düthmann, S. Vorogushyn, H. Kreibich, Drivers of flood risk change in residential areas, Nat. Hazards Earth Syst. Sci. 12 (2012) 1641–1657, https://doi.org/10.5194/nhess-12-1641-2012.
[15] H. Cammerer, A.H. Thieken, J. Lammel, Adaptability and transferability of flood loss functions in residential areas, Nat. Hazards Earth Syst. Sci. 13 (11) (2013) 3063–3081, https://doi.org/10.5194/nhess-13-3063-2013.
[16] Y. He, D. Manful, R. Warren, N. Forstenhäusler, T.J. Osborn, J. Price, R. Jenkins, C. Wallace, D. Yamazaki, Quantification of impacts between 1.5 and 4°C of global warming on flooding risks in six countries, Clim. Change 170 (1–2) (2022) 15, https://doi.org/10.1007/s10584-021-03289-5.
[17] T. Lazzarin, A. Defina, D.P. Viero, Assessing 40 years of flood risk evolution at the micro-scale using an innovative modeling approach: the effects of urbanization and land planning, Geosciences 13 (4) (2023) 112, https://doi.org/10.3390/geosciences13040112.
[18] P.B. Sayers, M. Horritt, S. Carr, A. Kay, J. Mauz, R. Lamb, E. Penning-Rowsell, Third UK Climate Change Risk Assessment (CCRA3): Future Flood Risk. Main Report - Final Report Prepared for the Committee on Climate Change, UK, Committee on Climate Change, London, 2020, p. 102 (UKCEH Project no. C07063).
[19] CH2M, A Flood Management High Level Review for the Broads Climate Partnership, Broads Authority, Norwich, 2016. Retrieved from, http://www.broads-authority.gov.uk/looking-after/climate-change/broads-community.

[20] U. Pasquier, R. Few, M.C. Goulden, S. Hooton, Y. He, K.M. Hiscock, "We can't do it on our own!"—Integrating stakeholder and scientific knowledge of future flood risk to inform climate change adaptation planning in a coastal region, Environ. Sci. Pol. 103 (2020) 50–57, https://doi.org/10.1016/j.envsci.2019.10.016.
[21] Environment Agency, Saline incursion on the Norfolk Broads - creating a better place, Retrieved from, https://environmentagency.blog.gov.uk/2022/12/02/saline-incursion-on-the-norfolk-broads/, 2022.
[22] Defra, Shoreline management plan guidance volume 1: aims and requirements, Retrieved from, https://assets.publishing.service.gov.uk/government/uploads/system/uploads/attachment_data/file/69206/pb11726-smpg-vol1-060308.pdf, 2006.
[23] Defra, Shoreline management plan guidance volume 2: procedures, Retrieved from, https://assets.publishing.service.gov.uk/media/5a75c748ed915d506ee8168d/pb11726v2-smpg-vol2-060523.pdf, 2006.
[24] Environment Agency, Kelling to Lowestoft Ness shoreline management plan, Retrieved from, https://environment.data.gov.uk/shoreline-planning/documents/SMP6%2FKelling%20to%20Lowestoft%20Ness%20SMP%20-%20final.pdf, 2012.
[25] S.A. Day, T. O'Riordan, J. Bryson, P. Frew, R. Young, Many stakeholders, multiple perspectives: Long-Term planning for a future Coast, in: R.J. Nicholls, R.J. Dawson, S.A. Day (Eds.), Broad Scale Coastal Simulation: New Techniques to Understand and Manage Shorelines in the Third Millennium, Springer, Dordrecht, 2015, pp. 299–323, https://doi.org/10.1007/978-94-007-5258-0_12.
[26] S. Hooton, Climate change adaptation plan, Retrieved from, https://www.broads-authority.gov.uk/_data/assets/pdf_file/0014/200651/Climate-Change-Adaptation-Plan.pdf, 2015.
[27] T. Thumerer, A.P. Jones, D. Brown, A GIS based coastal management system for climate change associated flood risk assessment on the east coast of England, Int. J. Geogr. Inf. Sci. 14 (3) (2000) 265–281, https://doi.org/10.1080/136588100240840.
[28] M. Mokrech, R.J. Nicholls, R.J. Dawson, Scenarios of future built environment for coastal risk assessment of climate change using a GIS-Based Multicriteria analysis, Environ. Plann. Plann. Des. 39 (1) (2012) 120–136, https://doi.org/10.1068/b36077.
[29] C.C. Shepard, V.N. Agostini, B. Gilmer, T. Allen, J. Stone, W. Brooks, M.W. Beck, Assessing future risk: quantifying the effects of sea level rise on storm surge risk for the southern shores of Long Island, New York, Nat. Hazards 60 (2) (2011) 727–745, https://doi.org/10.1007/s11069-011-0046-8.
[30] K. Garbutt, C. Ellul, T. Fujiyama, Mapping social vulnerability to flood hazard in Norfolk, England, Environ. Hazards 14 (2) (2015) 156–186, https://doi.org/10.1080/17477891.2015.1028018.
[31] S. Scheuer, D. Haase, V. Meyer, Exploring multicriteria flood vulnerability by integrating economic, social and ecological dimensions of flood risk and coping capacity: from a starting point view towards an end point view of vulnerability, Nat. Hazards 58 (2) (2010) 731–751, https://doi.org/10.1007/s11069-010-9666-7.
[32] I. Kotzee, B. Reyers, Piloting a social-ecological index for measuring flood resilience: a composite index approach, Ecol. Indic. 60 (2016) 45–53, https://doi.org/10.1016/j.ecolind.2015.06.018.
[33] Environment Agency, Broadland Rivers catchment flood management plan, Retrieved from, https://assets.publishing.service.gov.uk/government/uploads/system/uploads/attachment_data/file/288882/Broadland_Rivers_Catchment_Flood_Management_Plan.pdf, 2009.
[34] Broads Authority, Broadland Rivers catchment plan, Retrieved from, https://broadlandcatchmentpartnership.org.uk/wp-content/uploads/2018/08/Catchment-Plan-website-final.pdf, 2014.
[35] T. Giakoumis, N. Voulvoulis, Water Framework Directive programmes of measures: lessons from the 1st planning cycle of a catchment in England, Sci. Total Environ. 668 (2019) 903–916, https://doi.org/10.1016/j.scitotenv.2019.01.405.
[36] Office for National Statistics, Census 2021 geographies - Office for National Statistics, Retrieved from, https://www.ons.gov.uk/methodology/geography/ukgeographies/censusgeographies/census2021geographies, 2023.
[37] Broads Authority, Broads climate change adaptation plan report by head of strategy and projects, Retrieved from, https://www.broads-authority.gov.uk/_data/assets/pdf_file/0014/200651/Climate-Change-Adaptation-Plan.pdf, 2015.
[38] G. Mosby, The horsey flood, 1938: an example of storm effect on a low Coast, Geogr. J. 93 (5) (1939), https://doi.org/10.2307/1788711, 413–413.
[39] T. Spencer, S.M. Brooks, B.R. Evans, J.A. Tempest, I. Möller, Southern North Sea storm surge event of 5 December 2013: water levels, waves and coastal impacts, Earth Sci. Rev. 146 (2015) 120–145, https://doi.org/10.1016/j.earscirev.2015.04.002.
[40] Environment Agency, The costs and impacts of the winter 2013 to 2014 floods, Retrieved from, https://www.gov.uk/flood-and-coastal-erosion-risk-management-research-reports/the-costs-and-impacts-of-the-winter-2013-to-2014-floods, 2016.
[41] D. Matless, Checking the sea: geographies of authority on the East Norfolk Coast (1790–1932), Rural Hist. 30 (2) (2019) 215–240, https://doi.org/10.1017/s0956793319000207.
[42] U. Pasquier, Y. He, S. Hooton, M. Goulden, K.M. Hiscock, An integrated 1D–2D hydraulic modelling approach to assess the sensitivity of a coastal region to compound flooding hazard under climate change, Nat. Hazards 98 (3) (2018) 915–937, https://doi.org/10.1007/s11069-018-3462-1.
[43] U. Pasquier, Modelling Future Flood Risks for Inland and Coastal Adaptation Planning, PhD Thesis, University of East Anglia, Norwich, UK, 2020. Available from: the UEA Digital Repository, https://ueaeprints.uea.ac.uk/id/eprint/93979/1/PhD_2020_UlyssePasquier_Modelling%20future%20flood%20risks%20for%20inland%20and%20coastal%20adaptation%20planning%201.pdf.
[44] Y. He, D. Manful, N. Forstenhäusler, Y. Huang, B. Smith, Q. Zha, Escalating hydroclimatic extremes and volatility in the UK under 2°C and 4°C warming, Earths Future 14 (2026) e2025EF007156, https://doi.org/10.1029/2025EF007156.
[45] J.W. Hall, R.J. Dawson, P. Sayers, C. Rosu, J. Chatterton, R. Deakin, A methodology for national-scale flood risk assessment, Proceedings of the Institution of Civil Engineers - Water & Maritime Engineering 156 (3) (2003) 235–247, https://doi.org/10.1680/wame.2003.156.3.235, 2003.
[46] H. Booth, Demographic forecasting: 1980 to 2005 in review, Int. J. Forecast. 22 (3) (2006) 547–581, https://doi.org/10.1016/j.ijforecast.2006.04.001.
[47] S.N. Jonkman, P.H.A.J.M. Van Gelder, J.K. Vrijling, Loss of life models for sea and river floods, in: B. Wu, Z.Y. Wang, G.Q. Wang, G.H. Huang, J. Huang (Eds.), Flood Defence 2002: Proceedings of the Second International Symposium on Flood Defence, vol. 1, Science Press, New York, 2002, pp. 196–206.
[48] E. Penning-Rowsell, P. Floyd, D. Ramsbottom, S. Surendran, Estimating injury and loss of life in floods: a deterministic framework, Nat. Hazards 36 (1–2) (2005) 43–64, https://doi.org/10.1007/s11069-004-4538-7.
[49] I. Ruin, J.D. Creutin, S. Anquetin, C. Lutoff, Human exposure to flash floods – relation between flood parameters and human vulnerability during a storm of September 2002 in Southern France, J. Hydrol. 361 (1–2) (2008) 199–213, https://doi.org/10.1016/j.jhydrol.2008.07.044.
[50] T. Lazzarin, A.S. Chen, D.P. Viero, Beyond flood hazard: mapping the loss probability of pedestrians to improve risk estimation and communication, Sci. Total Environ. 912 (2024) 168718, https://doi.org/10.1016/j.scitotenv.2023.168718.
[51] G. Bernardini, F. Lagona, M. Mingione, et al., Probabilistic assessment of human instability in urban areas exposed to flood events, Sci. Rep. 15 (2025) 41505, https://doi.org/10.1038/s41598-025-25267-y.
[52] D. Ramsbottom, E.C. Penning-Rowsell, P. Floyd, Flood Risks to People: Phase 1. R&D Technical Report FD 2317, Department of the Environment, London, 2003. Food and Rural Affairs and Environment Agency, https://assets.publishing.service.gov.uk/media/602a8e2ae90e07055b9d3240/Flood_Risks_to_People_Phase_1_technical_report.pdf.
[53] Humanitarian Data Exchange (HDX), Retrieved from: https://data.humdata.org/dataset/united-kingdom-high-resolution-population-density-maps-demographic-estimates, 2026.
[54] T.G. Tiecke, X. Liu, A. Zhang, A. Gros, N. Li, G. Yetman, et al., Mapping the world population one building at a time, Retrieved from, https://arxiv.org/abs/1712.05839, 2017.
[55] K.S. Atwal, T. Anderson, Dieter Pfoser, A. Züfle, Predicting building types using OpenStreetMap, Sci. Rep. 12 (1) (2022), https://doi.org/10.1038/s41598-022-24263-w.
[56] Environment Agency, Framework and tools for local flood risk assessment: software user guide SC070059/R4, Retrieved from, https://assets.publishing.service.gov.uk/government/uploads/system/uploads/attachment_data/file/314649/Local_flood_risk_assessment_-_software_user_guide.pdf, 2014.
[57] E. Penning-Rowsell, C. Green, Enhanced appraisal of flood alleviation benefits, in: D.J. Parker (Ed.), Floods, Volume I: New Approaches and Lessons from Experience, Routledge, London and New York, 2000.

[58] K.M. de Bruijn, Resilience indicators for flood risk management systems of lowland rivers, Int. J. River Basin Manag. 2 (3) (2004) 199–210, https://doi.org/10.1080/15715124.2004.9635232.
[59] T. Gerl, H. Kreibich, G. Franco, D. Marechal, K. Schröter, A review of flood loss models as basis for harmonization and benchmarking, PLoS One 11 (7) (2016) e0159791, https://doi.org/10.1371/journal.pone.0159791.
[60] M. Pregnolato, C. Galasso, A compendium of existing vulnerability and fragility relationships for flood, AGU Fall Meeting Abstracts 2018 (2018) NH52B02.
[61] I. Bombelli, D. Molinari, P. Asaridis, F. Ballio, The "Flood Damage Models" repository. Proceedings of the 4th European Conference on Flood Risk Management (Floodrisk 2020), 2021, https://doi.org/10.3311/FloodRisk2020.11.3.
[62] J. Huizinga, H. De Moel, W. Szewczyk, Global Flood depth-damage Functions: Methodology and the Database with Guidelines, Joint Research Centre (Seville Site), 2017, https://doi.org/10.2760/16510.
[63] XE.com, XE currency converter - live rates, Retrieved from, https://www.xe.com/currencyconverter/, 2025.
[64] HM Treasury, GDP deflators at market prices, and money GDP, Retrieved from, https://www.gov.uk/government/collections/gdp-deflators-at-market-prices-and-money-gdp?form=MG0AV3, 2025.
[65] P.M. Kelly, W.N. Adger, Theory and practice in assessing vulnerability to climate change and facilitating adaptation, Clim. Change 47 (4) (2000) 325–352, https://doi.org/10.1023/a:1005627828199.
[66] S. Vyas, L. Kumaranayake, Constructing socio-economic status indices: how to use principal components analysis, Health Pol. Plann. 21 (6) (2006) 459–468, https://doi.org/10.1093/heapol/czl029.
[67] H.F. Kaiser, J. Rice, Little jiffy, mark Iv, Educ. Psychol. Meas. 34 (1) (1974) 111–117, https://doi.org/10.1177/001316447403400115.
[68] M.S. Bartlett, Tests of significance in factor analysis, Br. J. Stat. Psychol. 3 (2) (1950) 77–85, https://doi.org/10.1111/j.2044-8317.1950.tb00285.x.
[69] M. Saisana, S. Tarantola, State-Of-The-Art Report on Current Methodologies and Practices for Composite Indicator Development, 214, 2002, pp. 4–15, https://doi.org/10.13140/RG.2.1.1505.1762.
[70] H. Eakin, A.L. Luers, Assessing the vulnerability of social-environmental systems, Annu. Rev. Environ. Resour. 31 (1) (2006) 365–394, https://doi.org/10.1146/annurev.energy.30.050504.144352.
[71] E. Penning-Rowsell, S. Priest, D. Parker, J. Morris, S. Tunstall, C. Viavattene, et al., Flood and Coastal Erosion Risk Management: a Manual for Economic Appraisal, Routledge, London, 2013, https://doi.org/10.4324/9780203066393.
[72] J.H. Kwakkel, M. Haasnoot, W.E. Walker, Comparing Robust Decision-Making and Dynamic Adaptive Policy Pathways for model-based decision support under deep uncertainty, Environ. Model. Software 86 (2016) 168–183, https://doi.org/10.1016/j.envsoft.2016.09.017.
[73] H.R. Maier, J.H.A. Guillaume, H. van Delden, G.A. Riddell, M. Haasnoot, J.H. Kwakkel, An uncertain future, deep uncertainty, scenarios, robustness and adaptation : how do they fit together? Environ. Model. Software 81 (2016) 154–164, https://doi.org/10.1016/j.envsoft.2016.03.014.
[74] M. Workman, G. Darch, K. Dooley, G. Lomax, J. Maltby, H. Pollitt, Climate policy decision making in contexts of deep uncertainty—From optimisation to robustness, Environ. Sci. Pol. 120 (2021) 127–137, https://doi.org/10.1016/j.envsci.2021.03.002.
[75] S. Surminski, Business and industry, in: R.A. Betts, A.B. Haward, K.V. Pearson (Eds.), The Third UK Climate Change Risk Assessment Technical Report, Prepared for the Climate Change Committee, London, 2021. https://www.ukclimaterisk.org/wp-content/uploads/2021/06/Technical-Report-The-Third-Climate-Change-Risk-Assessment.pdf.
[76] J.H. Kwakkel, E. Pruyt, Exploratory Modeling and Analysis, an approach for model-based foresight under deep uncertainty, Technol. Forecast. Soc. Change 80 (3) (2013) 419–431, https://doi.org/10.1016/j.techfore.2012.10.005.
[77] N.S. Entwistle, G.L. Heritage, L.A. Schofield, R.J. Williamson, Recent changes to floodplain character and functionality in England, Catena 174 (2019) 490–498, https://doi.org/10.1016/j.catena.2018.11.018.
[78] G. Heritage, N.S. Entwistle, The impact of floodplain degradation on flooding in the UK, in: *Proceedings of the 37th IAHR World Congress*, 13–18 August 2017, Kuala Lumpur, Malaysia, International Association for Hydro-Environment Engineering and Research, 2017.
[79] T. Orusa, A. Viani, B. Moyo, D. Cammareri, E.B. Mondino, Risk assessment of rising temperatures using landsat 4–9 LST time series and meta® population dataset: an application in Aosta Valley, NW Italy, Remote Sens. 15 (9) (2023), https://doi.org/10.3390/rs15092348, 2348–2348.
[80] C.D. Dziuban, E.C. Shirkey, When is a correlation matrix appropriate for factor analysis? Some decision rules, Psychol. Bull. 81 (6) (1974) 358–361, https://doi.org/10.1037/h0036316.
[81] V. Meyer, S. Scheuer, D. Haase, A multicriteria approach for flood risk mapping exemplified at the Mulde river, Germany, Nat. Hazards 48 (1) (2009) 17–39, https://doi.org/10.1007/s11069-008-9244-4.
[82] S. Kienberger, S. Lang, P. Zeil, Spatial vulnerability units – expert-based spatial modelling of socio-economic vulnerability in the Salzach catchment, Austria, Nat. Hazards Earth Syst. Sci. 9 (3) (2009) 767–778, https://doi.org/10.5194/nhess-9-767-2009.
[83] M. Gall, Indices of Social Vulnerability to Natural Hazards: a Comparative Evaluation (Phd Thesis), University of South Carolina, Columbia, SC, USA, 2007.
[84] T. Wu, Quantifying coastal flood vulnerability for climate adaptation policy using principal component analysis, Ecol. Indic. 129 (2021) 108006, https://doi.org/10.1016/j.ecolind.2021.108006.
[85] V. Uddameri, E.A. Hernandez, Machine learning for flood Resiliency—Current status and unexplored directions, Environments 12 (8) (2025) 259, https://doi.org/10.3390/environments12080259.
[86] C.M. Fontaine, M. Mokrech, M.D.A. Rounsevell, Land use dynamics and coastal management, Adv. Clim. Change Res. (2015) 125–146, https://doi.org/10.1007/978-94-007-5258-0_4.
[87] D. King, Uses and limitations of socioeconomic indicators of community vulnerability to natural hazards: data and disasters in Northern Australia, Nat. Hazards 24 (2001) 147–156.
[88] C. Yepes-Estrada, A. Calderon, C. Costa, H. Crowley, J. Dabbeek, Maria Camila Hoyos, et al., Global building exposure model for earthquake risk assessment, Earthq. Spectra 39 (4) (2023) 2212–2235, https://doi.org/10.1177/87552930231194048.
[89] D. Schorlemmer, T. Beutin, F. Cotton, Ospina Nicolas Garcia, N. Hirata, Kuo Fong Ma, et al., Global dynamic exposure and the OpenBuildingMap - a big-data and crowd-sourcing approach to exposure modeling. https://doi.org/10.5194/egusphere-egu2020-18920, 2020.
[90] L. Liu, X. Cao, S. Li, N. Jie, A 31-year (1990–2020) global gridded population dataset generated by cluster analysis and statistical learning, Sci. Data 11 (1) (2024) 124, https://doi.org/10.1038/s41597-024-02913-0.
[91] M. Pesaresi, Schiavina Marcello, P. Politis, S. Freire, Katarzyna Krasnodębska, J.H. Uhl, et al., Advances on the global human settlement layer by joint assessment of earth observation and population survey data, Int. J. Digit. Earth 17 (1) (2024), https://doi.org/10.1080/17538947.2024.2390454.
[92] Worldpop, WorldPop, Retrieved from, https://www.worldpop.org/, 2025.
[93] H. Wu, M. Zhang, Y. He, P. Chen, U. Pasquier, H. Hu, J. Wen, Scenario-based flood adaption of a fast-developing delta city: modeling the extreme compound flood adaptations for Shanghai, Int. J. Disaster Risk Reduct. 117 (2025) 105207, https://doi.org/10.1016/j.ijdrr.2025.105207.
[94] R. Warren, O. Andrews, S. Brown, F.J. Colón-González, N. Forstenhäusler, D.E.H.J. Gernaat, P. Goodwin, I. Harris, Y. He, C. Hope, D. Manful, T.J. Osborn, J. Price, D. van Vuuren, R.M. Wright, Quantifying risks avoided by limiting global warming to 1.5 or 2°C above pre-industrial levels, Clim. Change 172 (3–4) (2022) 39, https://doi.org/10.1007/s10584-021-03277-9.
[95] O. Butters, C. Robson, F. McClean, V. Glenis, J. Virgo, A. Ford, et al., An open framework for analysing future flood risk in urban areas, Environ. Model. Software 185 (2025) 106302, https://doi.org/10.1016/j.envsoft.2024.106302.
[96] Z. Yin, Y. Hu, K. Jenkins, Y. He, N. Forstenhäusler, R. Warren, L. Yang, R. Jenkins, D. Guan, Assessing the economic impacts of future fluvial flooding in six countries under climate change and socio-economic development, Clim. Change 166 (3–4) (2021) 38, https://doi.org/10.1007/s10584-021-03059-3.

[97] T. Lazzarin, D.P. Viero, D. Molinari, F. Ballio, A. Defina, Flood damage functions based on a single physics- and data-based impact parameter that jointly accounts for water depth and velocity, J. Hydrol. 607 (2022) 127485, https://doi.org/10.1016/j.jhydrol.2022.127485.
[98] D.P. Adeke, S.N. Mugume, A methodology for development of flood-depth-velocity damage functions for improved estimation of pluvial flood risk in cities, J. Hydrol. (2025) 132736, https://doi.org/10.1016/j.jhydrol.2025.132736.
[99] S. Wade, D. Ramsbottom, P. Floyd, E.C. Penning-Rowsell, S. Surendran, Risks to people: developing new approaches for flood hazard and vulnerability mapping, in: Defra Flood and Coastal Management Conference 2005, 2005, 5 - 7 July 2005, York, UK. Retrieved from, https://eprints.hrwallingford.com/562/.